



0021-9290(94)E0008-Q

## TECHNICAL NOTE

## A NEW OPTICAL SYSTEM FOR THE DETERMINATION OF DEFORMATIONS AND STRAINS: CALIBRATION CHARACTERISTICS AND EXPERIMENTAL RESULTS

K. A. DERWIN,\* L. J. SOSLOWSKY,\*† W. D. K. GREEN\*‡ and S. H. ELDER\*

\*Orthopaedic Research Laboratories; and †Center for Human Growth and Development, University of Michigan, Ann Arbor, MI 48109-0486, U.S.A.

**Abstract**—Many types of optical strain measurement systems have been used for the determination of deformations and strains in soft biological tissues. The purpose of this investigation is to report a new optical strain measurement system developed in our laboratory which offers distinct advantages over systems developed in the past. Our optical strain system has demonstrated excellent performance in calibration and experimental tests. Calibration tests illustrate the system's accuracy to 0.05% strain at 3.52% strain and 0.18% strain at 11.74% strain. Further, this system can measure strains to within 2% measurement error for strains in a 0–11.74% range when 100  $\mu\text{m}$  increments of motion are used for calibration. The resolution of our system appears to be at least as good as the linear micrometer (2  $\mu\text{m}$ ) used as a calibrating standard. Errors in strain measurement due to whole specimen rotation or translation are quantified. Rotations about an in-plane axis perpendicular to the direction of strain and translations in/out of the plane of focus result in the largest sources of error. Finally, in an *in vitro* biomechanical study of the rabbit Achilles tendon, experimental failure strains are  $4.3 \pm 0.9\%$  using this system.

## INTRODUCTION

Previous biomechanical studies on isolated soft biological tissues have utilized two fundamental approaches for measurement of strain: direct contact systems and optical systems. Direct contact systems involve attaching a transducer to the tissue during a mechanical test. Many types of displacement transducers are commonly used. These include but are not limited to liquid metal strain gages (e.g. Edwards *et al.*, 1970; Kennedy *et al.*, 1977; Monahan *et al.*, 1984), the Hall effect strain transducer (Arms *et al.*, 1983), and implantable types such as the differential variable reluctance transducer (Ray *et al.*, 1993). Such transducers generate an analog voltage which is related to displacement in the region of tissue to which the transducer has been attached. Optical strain measurement systems in various forms have also been used by many investigators (e.g. Butler *et al.*, 1984; Lanir and Fung, 1974; Vanderby *et al.*, 1991; Woo *et al.*, 1976, 1983; Yamamoto *et al.*, 1992). These systems involve the application of stain lines perpendicular to the loading axis of the tissue. The marked tissue section is then imaged during a mechanical test and images corresponding to discrete points in time are analyzed and compared to the initial reference image to determine tissue strain.

The purpose of the current investigation is to report a new optical strain measurement system developed in our laboratory. A detailed description of the new system, comparisons to existing optical systems including potential advantages and disadvantages, a carefully performed calibration experiment, and an initial application to the Achilles tendon of the rabbit will be presented.

## MATERIALS AND METHODS

*The optical strain system*

The optical system implemented in this study consists of a Cohu 4810 Series video camera and Fujinon 10–140 mm zoom lens with a 2 $\times$  extender, a Panasonic AG-7500A video cassette recorder (VCR), and a BCD-5000 video controller which is interfaced to a Macintosh microcomputer (see Fig. 1). The video controller writes Society of Motion Picture

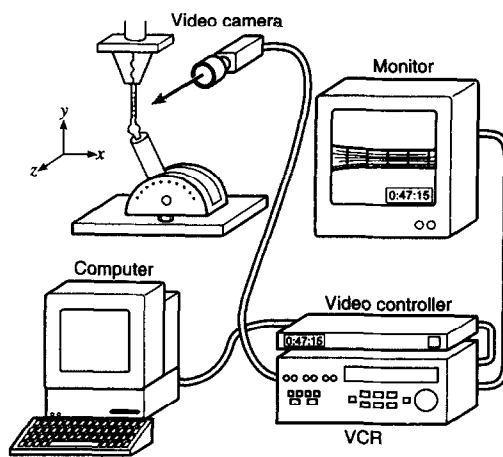


Fig. 1. Schematic of the optical strain system used to record uniaxial tensile strains in soft biological tissues such as tendon or ligament. Note that the specimen is aligned such that the direction of strain is actually along the vertical *y*-axis. Hence the camera is positioned on its side during a test such that the direction of strain appears horizontal on the monitor allowing for maximum resolution of the digitized images.

Received in final form: 10 January 1994.

† Author to whom correspondence should be addressed at: Orthopaedic Research Laboratories, University of Michigan, Ann Arbor, MI 48109-0486, U.S.A.

and Television Engineers (SMPTE) time-code on the audio channel of standard videotape, thereby allowing an extremely precise time-synchronized record of all tests. The frequency of the time-coded tape is 30 frames per second. The time-code allows *exact* frame addressing on the videotape, providing temporally perfect and clean frame grabbing ability during post-processing analysis.

This system is used to optically record mechanical tests. The test specimen is mounted in a fixture and reference lines are applied with tissue stain. The camera is manually aligned with the test specimen and remains fixed throughout an entire experimental test (see Fig. 1). If the specimen is oriented such that the direction of strain is along the global vertical axis (such as in the uniaxial tensile test shown in Fig. 1), the camera is first positioned on its side prior to alignment. Positioning the camera on its side for these types of tests causes the direction of strain to appear horizontal on the monitor, allowing for maximum resolution of the digital image. Computer software is then implemented which synchronizes the beginning of a mechanical test, the start of computer acquisition of experimental data such as load, and the first frame of recorded video. During the course of the test, load-time and deformation-time are recorded simultaneously, both having the same reference point in real time.

Following an experimental test, strain determination is achieved by several post-processing steps. Frames corresponding to designated points in time are digitized using specially written software and a frame grabbing board in the microcomputer. These 256 level gray-scale images show a section of the tissue with stain lines approximately perpendicular to the direction of uniaxial stretching. For each image, a region over which strain measurements will be made is selected by the analyst. Any region on the image may be selected as long as it includes at least two stain lines, and the orientation of this region should represent the direction of strain in the tissue. The region of interest may be the whole tissue surface or any subregion of the tissue over which strain measurements are desired such as a particular band of a tendon or ligament. The region of interest for a group of images from a single test is typically selected by looking at images from the end of a test and selecting the largest area which includes reference lines without significant breaks. Anatomical landmarks on the tissue or artificial landmarks from small stain marks randomly placed near the ends of the tissue may be used to aid the analyst in selecting the same region on each image. Hence, the same region of interest is selected on all images from a given test, even though the reference stain lines may shift during the test. Although this last step is manual, it allows for selecting the same portion of tissue for strain analysis on all images even though the size and orientation of the region may vary.

The strain analysis algorithm was written in C for a UNIX and X windows environment. The program takes as input the designated region of interest on each image and the direction in which to measure strain. The image processing is completely automated and proceeds as a series of steps. First, the image is smoothed to eliminate banding or other artifacts. Smoothing also makes the image cleaner, although less sharp, which makes the subsequent processing easier by preventing small breaks in stain line edges which might otherwise interfere with the analysis. The smoothing is performed by convolving the image intensity with the Gaussian  $f(x) = \exp(-ax^2)$ , where  $a$  is a constant which is chosen based on image quality. Second, the gradient of the smoothed image is calculated in the direction of strain. This is the simplest way of detecting the edges of the stain lines which are nearly perpendicular to the direction of strain. Third, the gradient is thresholded to give areas of positive and negative slope (corresponding to the left and right edges of the lines and also of other tissue nonuniformities). The stain lines are detected by discarding all areas which do not span the full width of the region of interest. Fourth, the gradient is sampled along scan lines (corresponding to rows of pixels)

parallel to the direction of strain and the intersection with each edge of a stain line is estimated by taking a weighted average of the positions with highest slope. This is preferred to taking the single position with greatest slope since it avoids the discontinuity occurring when there is not a single peak in the slope. Last, the positions of the left and right edges of each stain line are averaged to give a position for each line. Comparing these positions between images gives the apparent strain between images. An example of the steps performed on a single digitized frame from the test of a rabbit Achilles tendon is displayed in Fig. 2.

#### Calibration tests

To assess the calibration characteristics of our optical system, two types of tests were performed. The first type of test determined the system's ability to accurately measure in-plane uniaxial deformations. The second type of test determined the errors introduced in the optical measures due to whole specimen translation or rotation during an experimental test.

Two calibration blocks  $38.10 \times 40.60$  mm ( $\pm 12.70$   $\mu$ m) were manufactured for the calibration tests (see Fig. 3). A grid consisting of parallel sets of horizontal and vertical lines 0.2540 mm (0.0100 in.) thick and 12.70 or 25.40 mm apart was printed on a 2540 dots per inch Linotronic Imagesetter and fixed to each of the blocks. These distances between lines are representative of typical experimental gage lengths. Error in line thickness and distance between lines on the grid is estimated to be less than 2.540  $\mu$ m, while errors in perfect alignment of the grid on the block are likely  $\pm 25.4$   $\mu$ m linearly and  $< 0.5^\circ$  rotationally. The calibration blocks were mounted on either a linear micrometer/stage fixture or a computer numeric control (CNC) milling machine depending on the type of test. The linear micrometer has a resolution of 2  $\mu$ m and moves a single degree-of-freedom stage. The CNC has a resolution of 25.4  $\mu$ m (0.001 in.) and is capable of linear translation in three orthogonal directions.

Several performance characteristics of the optical system were evaluated in addition to the specific calibration parameters that are outlined in detail for each test below. For each calibration test, the effects of camera-to-object distance and a close-up lens were evaluated. To evaluate the effects of camera-to-object distance and a close-up lens, all tests were run at two different camera-to-object distances. First, using an additional close-up lens, the camera was positioned at a distance from the blocks (50–55 cm) so that lines representing a 12.70 mm reference distance could be magnified to fill the field of view. Secondly, without the close-up lens, the camera was repositioned at a distance from the blocks (100–115 cm) so that lines representing the 25.40 mm reference distance could be magnified to fill the field of view. The maximum magnification of the zoom lens was not used in either case. Also, within the following sets of calibration tests, lighting, lens  $f$ -stop setting, and optical distortion from liquid and glass were evaluated. The details of each set of calibration tests are given below.

(a) *Test series 1: linear, in-plane, uniaxial translation using two blocks.* The first series of tests consisted of linear, in-plane, uniaxial translation using two blocks moving with respect to each other along the vertical  $y$ -axis (see Fig. 1). One block was mounted on the vertically oriented micrometer stage so that it was square with and opposed to the second block which was fixed below it on the table. In this position, the bottommost horizontal lines on the upper block were very close to 12.7 and 25.4 mm from the topmost horizontal lines on the lower block. The exact initial gage length was obtained from the known distance between two lines on the same block and pixel distances between both the known lines and the gage lines (calculated from an initial digitized image). With one block fixed, the other block was vertically translated with respect to the first block 0.900 mm in 20  $\mu$ m increments and then incrementally back to the starting

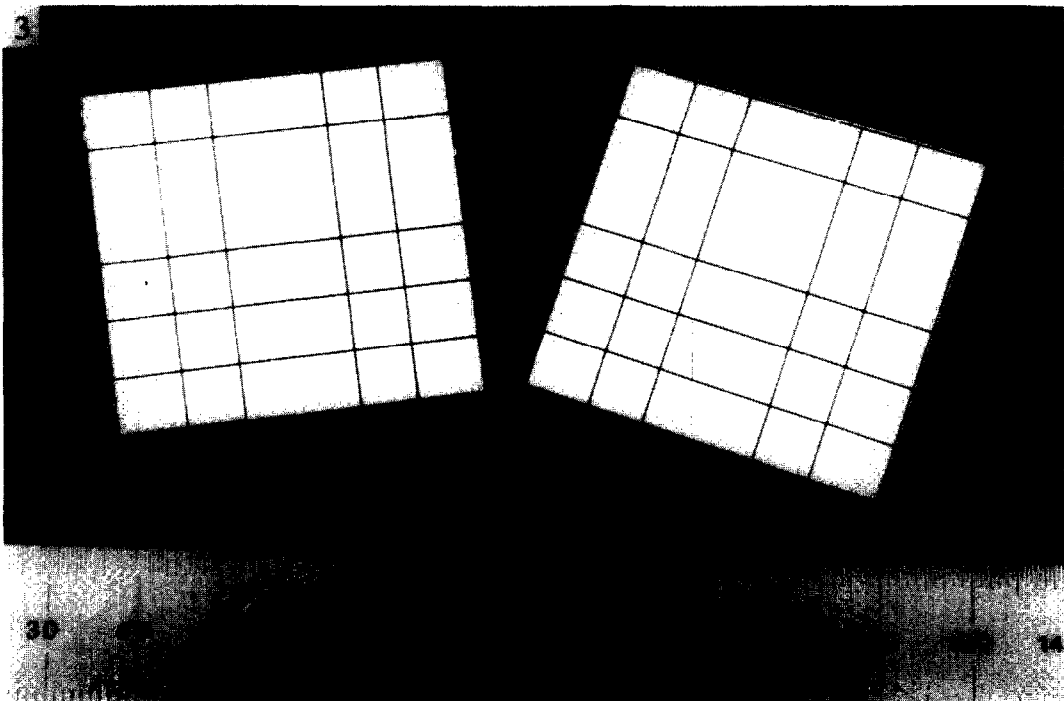
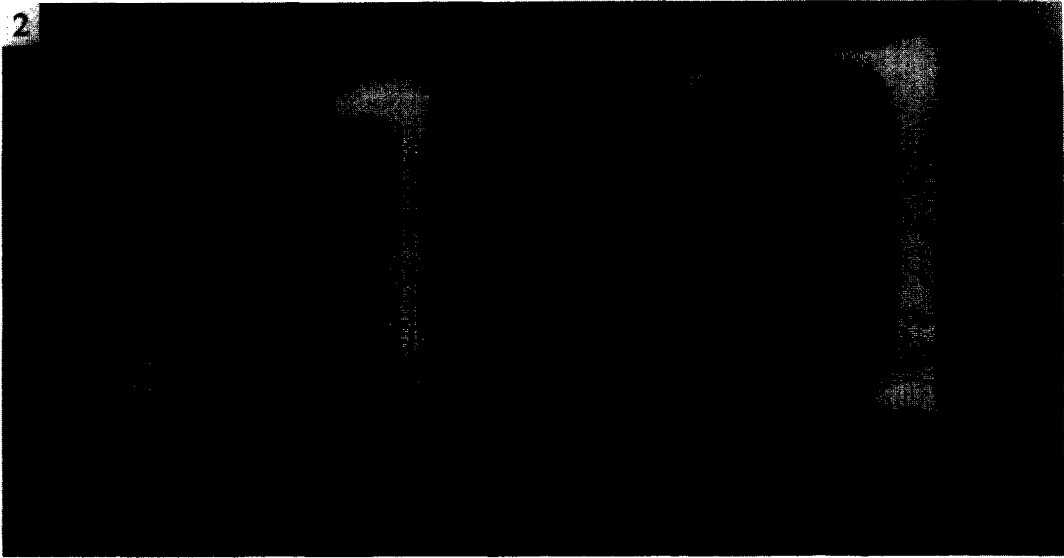


Fig. 2. Digital image of tendon following optical strain analysis.

Fig. 3. Calibration blocks affixed with high-resolution grid lines and used for calibration tests of the optical strain system (scale in mm).



position. This movement represented  $\sim 3.5\%$  'strain' with respect to the larger gage length. Next, with one block fixed, the other block was vertically translated with respect to the first block 3.000 mm in 100  $\mu\text{m}$  increments and then incrementally back to the starting position. This movement represented  $\sim 11.7\%$  'strain' with respect to the larger gage length. The micrometer motion was used to define the actual motion of the two blocks as they were moved apart from each other and hence the actual motion of two parallel grid lines as they moved with respect to each other. Both of these tests were also repeated with the calibration blocks submersed in a glass tank of circulating physiologic saline solution.

A percent actual strain was calculated as the actual (micrometer) motion divided by the initial gage length. Optical strain was determined by the analysis software. The difference between actual and optical strain was used to estimate error in the optical system. A percent measurement error for the optical system was then calculated as the difference between the optical and actual strains divided by the actual strain. Further, differences between the optical and actual strains during each increment of motion were used to evaluate the resolution of the optical system as well as the potential bias of the system toward over- or underestimating actual motions. The actual incremental strain was calculated as the increment of actual motion divided by the initial gage length, while optical incremental strain was determined by the analysis software. Note that actual incremental motion was either 20 or 100  $\mu\text{m}$  in this test series.

(b) *Test series 2: Uniaxial translations of one block.* The second calibration test series consisted of uniaxial translations of a single calibration block. The block was mounted on the CNC and moved along each of its three orthogonal  $x$ -,  $y$ - and  $z$ -axes while tracking two vertical gage lines (see reference axes, Fig. 1). The first test was side-to-side translation (along the  $x$ -axis)  $\pm 6.35$  mm by 1.27 mm increments. The second test involved vertical translation (along the  $y$ -axis)  $\pm 6.35$  mm by 1.27 mm increments. The third test was translation in/out of the plane of focus (along the  $z$ -axis)  $\pm 12.7$  mm by 1.27 mm increments. This third test was repeated using three different  $f$ -stop and external lighting combinations. Since the distance between the vertical gage lines on the calibration block was constant, there was no actual strain occurring. A percent apparent optical strain was calculated, however, as the optical strain measured as a result of whole specimen translation during a test. These apparent optical strains represent errors in the optical measures.

(c) *Test series 3: rotations of one block.* The third calibration test series consisted of rotations of a single calibration block about each of its three orthogonal  $x$ -,  $y$ - and  $z$ -axes while tracking two vertical gage lines (see reference axes, Fig. 1). The block was mounted on the CNC machine, and National Bureau of Standards angle blocks were positioned between the block and a flat plate to obtain rotations accurate to 0.006°. The first test involved rotation about the horizontal  $x$ -axis  $\pm 10.00^\circ$  by 5.00° increments. The second test was rotation about the vertical  $y$ -axis  $\pm 10.00^\circ$  by 5.00° increments. The third test involved rotation about the  $z$ -axis  $\pm 30.00^\circ$  by 5.00° increments. Since the distance between the vertical gage lines on the calibration block was again constant, there was no actual strain occurring. A percent apparent optical strain was calculated however, as the optical strain measured as a result of whole specimen rotation during a test. These apparent optical strains represent errors in the optical measures.

#### Experimental in vitro biomechanical tests

An initial *in vitro* biomechanical study was completed using the optical strain system as an analysis tool. The experiment consisted of constant strain rate tensile tests to failure at 0.1%  $\text{s}^{-1}$  of eight Achilles tendons obtained from four mature New Zealand white rabbits. The calcaneus was

potted in a cylindrical pot, and the soft tissue was held by sinusoidal grips. The tendon cross-section was measured using an area micrometer similar to one described previously (Butler *et al.*, 1984). Reference lines were placed on the specimen perpendicular to the axis of testing using Verhoeff's stain. The specimen was then mounted in a physiologic saline bath and tested on an MTS servo-hydraulic testing machine. The optical system was used to quantify tissue strain.

## RESULTS

### Calibration tests

(a) *Test series 1: Linear, in-plane, uniaxial translation using two blocks.* The difference between the strain measured by the optical system ( $\epsilon_{\text{optical}}$ ) and the actual (micrometer) strain ( $\epsilon_{\text{mic}}$ ) when translating the blocks 0.900 mm with respect to each other (by 20  $\mu\text{m}$  increments) and for the further camera-to-object distance is shown in Fig. 4(a). The calculated initial gage length was 25.55 mm. The average of the absolute values of the differences between the micrometer and optically measured strain is  $0.021 \pm 0.013\%$  strain over a range of 0–3.52% strain, and the average of the absolute values of the measurement errors is  $1.327 \pm 0.92\%$ . At 3.52% strain, the optical system is accurate to 0.05% strain corresponding to 1.4% measurement error. Even at very small strains on the order of one increment of motion ( $\sim 0.08\%$  strain), the optical system is accurate to within 0.006% strain corresponding to about 8% measurement error.

Figure 4(b) depicts the differences between *incremental* strains measured by the optical system ( $\Delta\epsilon_{\text{optical}}$ ) and imposed by the micrometer ( $\Delta\epsilon_{\text{mic}}$ ) for a 0.900 mm translation of one block with respect to the other by 20  $\mu\text{m}$  ( $\sim 0.08\%$  strain) increments and for the further camera-to-object distance. The average of the absolute values of the differences between these incremental strains is  $0.004 \pm 0.003\%$ .

The difference between the strain measured by the optical system ( $\epsilon_{\text{optical}}$ ) and the actual (micrometer) strain ( $\epsilon_{\text{mic}}$ ) when translating the blocks 3.000 mm with respect to each other (by 100  $\mu\text{m}$  increments) and for the further camera-to-object distance is shown in Fig. 5(a). The calculated initial gage length was 25.55 mm. The average of the absolute values of the differences between the micrometer and optically measured strain is  $0.082 \pm 0.053\%$  strain over a range of 0–11.74% strain, and the average of the absolute values of the measurement errors is  $1.354 \pm 0.230\%$ . At 11.74% strain, the optical system is accurate to 0.18% strain corresponding to 1.6% measurement error. Even at small strains on the order of one increment of motion ( $\sim 0.4\%$  strain), the optical system remains accurate to within 2% measurement error.

Figure 5(b) depicts the differences between *incremental* strains measured by the optical system ( $\Delta\epsilon_{\text{optical}}$ ) and imposed by the micrometer ( $\Delta\epsilon_{\text{mic}}$ ) for a 3.000 mm translation of one block with respect to the other by 100  $\mu\text{m}$  ( $\sim 0.4\%$  strain) increments and for the further camera-to-object distance. The average of the absolute values of the differences between these incremental strains is  $0.007 \pm 0.005\%$ .

Although not shown in figure, form, the performance of the optical system was unaffected by imaging through the glass and circulating saline bath. Additionally, the results of these tests and those in all other test series show the optical system performed as well or better at the further camera-to-object distance. Hence, unless specifically relevant, only the results from the further camera-to-object distance will be reported.

(b) *Test series 2: uniaxial translations of one block.* The second series of calibration tests consisted of uniaxial translations of one block in all three orthogonal directions. Since the distance between the vertical gage lines on the block was constant, no actual strain occurred. Figure 6(a) shows, however, the percent apparent strain measured optically as a result of the block moving in the field of view. If 0.2% strain is

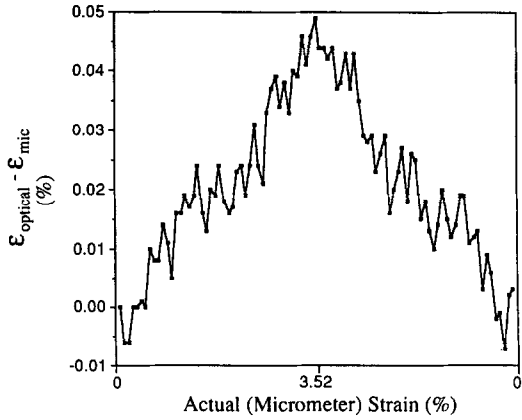


Fig. 4(a). Difference between optical and micrometer strain when imaging through air. Each increment of motion was  $20 \mu\text{m}$  ( $\sim 0.08\%$  strain), and the initial gage length was 25.55 mm.

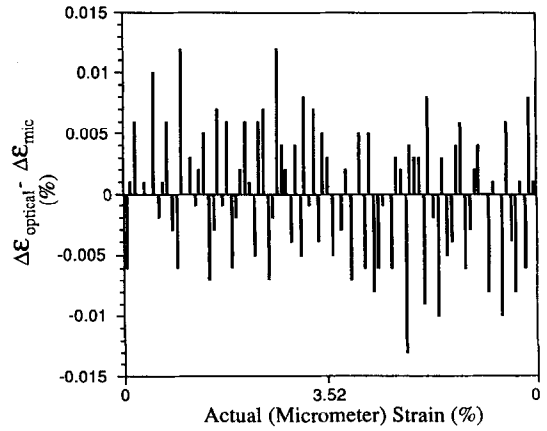


Fig. 4(b). Difference between optical and micrometer strain for each incremental movement when imaging through air. Each increment of motion was  $20 \mu\text{m}$  ( $\sim 0.08\%$  strain), and the initial gage length was 25.55 mm.

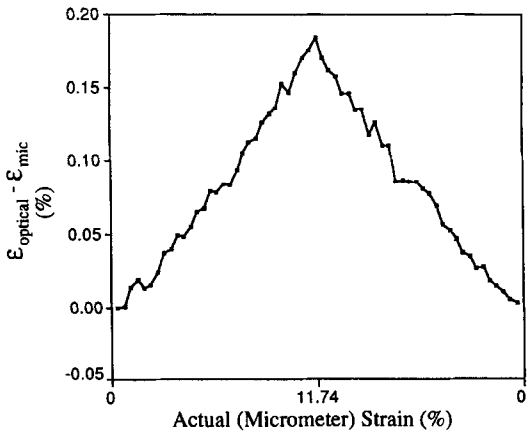


Fig. 5(a). Difference between optical and micrometer strain when imaging through air. Each increment of motion was  $100 \mu\text{m}$  ( $\sim 0.4\%$  strain), and the initial gage length was 25.55 mm.

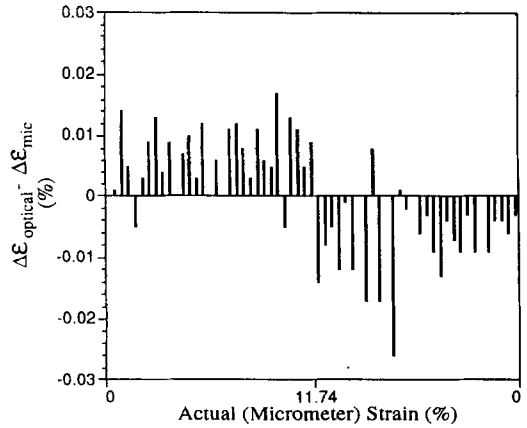


Fig. 5(b). Difference between optical and micrometer strain for each incremental movement when imaging through air. Each increment of motion was  $100 \mu\text{m}$  ( $\sim 0.4\%$  strain), and the initial gage length was 25.55 mm.

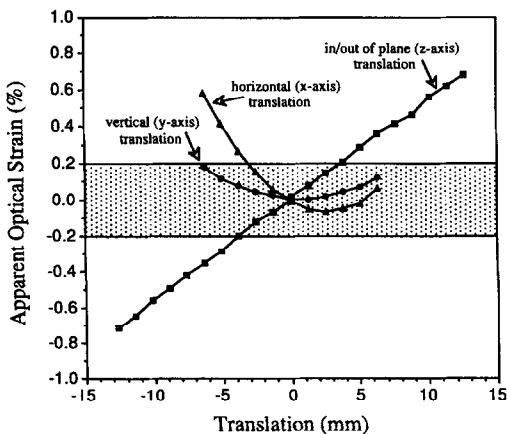


Fig. 6(a). Apparent optical strain vs linear translation of a single calibration block with a fixed gage length of 25.40 mm.

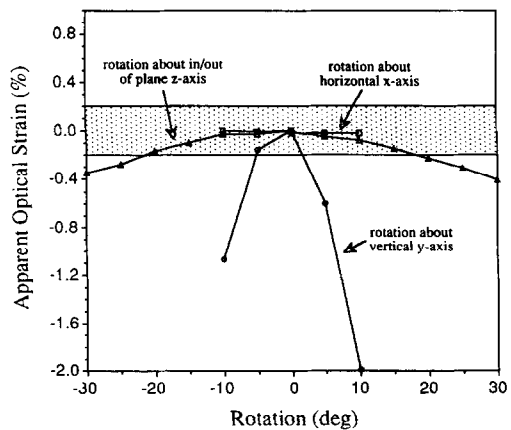


Fig. 6(b). Apparent optical strain vs rotation of a single calibration block with a fixed gage length of 25.40 mm.

used as an upper bound of acceptable error, Fig. 6(a) provides the acceptable range of linear motion for a specimen during a test. Note that the curve of horizontal translation along the  $x$ -axis vs apparent strain is not symmetric. These results confirm earlier tests indicating that the optical center of the lens is not in its geometric center (see the Discussion section). Although not shown graphically, it is noteworthy that the acceptable range of motion along the  $z$ -axis (i.e. the axis in/out of the plane of focus) is considerably less at the closer camera-to-object distance (approximately  $\pm 2.5$  mm vs  $\pm 3.8$  mm). The effects of lighting and lens  $f$ -stop on the results of linear motion along the  $z$ -axis in/out of the plane of focus are insignificant over a range of  $f/4$  to  $f/16$ .

(c) *Test series 3: rotations of one block.* The third series of calibration tests consisted of rotations of one block about the three orthogonal axes shown in Fig. 1. Since the distance between the vertical gage lines on the block was again constant, no actual strain occurred. Figure 6(b) shows, however, the percent apparent strain measured optically as a result of the block rotating in the field of view. If 0.2% strain is used as an upper bound of acceptable error, Fig. 6(b) provides the acceptable range of rotation for a specimen during a test. Note that the system is most sensitive to rotations about the vertical  $y$ -axis (i.e., the in-plane axis perpendicular to the direction of strain).

#### Experimental *in vitro* biomechanical tests

The results from the biomechanical *in vitro* study of rabbit Achilles tendons are reported in Table 1. Stress-strain curves demonstrated the toe, linear and failure regions typical of soft tissues. In particular, note that failure strains were  $4.3 \pm 0.9\%$  when using the optical system to quantify deformations. Five clamp-tendon-bone units failed by bone breakage at the calcaneus, and the remaining three by tendon substance rupture near the clamp.

### DISCUSSION

Optical techniques have been used by many investigators for the determination of strain in soft biological tissues. The most extensively used system is the video dimensional analyzer (VDA) system initially described by Yin *et al.* (1972) and Intaglietta and Tompkins (1972). The VDA has been used to experimentally measure surface strains during *in vitro* loading of articular cartilage (Woo *et al.*, 1976), ligaments and tendons (Woo, 1982; Woo *et al.*, 1983; Yamamoto *et al.*, 1992), and skin (Lanir and Fung, 1974). Other video/photographic noncontacting methods have been employed to measure strain. Roth and Mow (1980) photographed articular cartilage specimens and measured dimensional changes from the film negatives using a stereomicroscope-dial indicator method. High-speed video recording has been used to monitor tensile tests of human ligament, tendon, and fascia (Butler *et al.*, 1984; Noyes *et al.*, 1984; Zernicke *et al.*, 1984). Butler *et al.* (1990) used low-speed photography to measure surface strain variation in patellar tendon and knee cruciate ligaments. Vanderby *et al.* (1991) used a general optical system for strain evaluation on the femoral-MCL-tibia complex. Amadio *et al.* (1992) report tracking tissue markers on film and digitizing their position using a light board. Lee and

Danto (1992) presented a high-speed, high-resolution video digitizing system to track the motion of markers in two directions. Finally, the technique described in this paper has been used in our laboratory to measure strains in the human coracoacromial ligament (Soslowsky *et al.*, 1993) as well as in the rabbit Achilles tendon.

There are several issues common to all of the above techniques, including our own, that must be assessed when developing and utilizing an optical system. Radial distortion and a geometrically decentered optical center, even in a lens of extremely high quality, are two common sources of error. Current results from our system demonstrate that apparent strains develop due to simple linear motion as the edges of the field of view are approached. This is likely the result of radial distortion in the lens. In addition, the asymmetry of the apparent strains along a horizontal axis suggested that the optical center was not in the geometric center of the lens but skewed slightly to the left. In a separate analysis, this decentered distortion amounted to several pixels at the edge of the image. Further analysis using a fine calibration grid will provide a quantification of these effects. The analysis software will then be modified to incorporate appropriate corrections. In addition, camera positioning which encompasses alignment, camera-to-object distance, and magnification is a critical component in the accurate implementation of an optical system. The camera should be placed square to the object and as far from it as possible while still maintaining adequate magnification. Finally, tissue illumination must be considered. Diffuse lighting minimizes glare and shadows and increases contrast between the stain lines and the tissue. In general, for nonidealized experimental tests where the surface of the tissue is not perfectly smooth, lighting should be adjusted to utilize a higher lens  $f$ -stop, thereby providing increased depth of field.

The results presented for tracking linear in-plane motion demonstrate our system's ability to accurately measure in-plane uniaxial strains. At strains in the 0–3.52% range which were achieved by 20  $\mu$ m incremental motion, our system provided results that were typically about 1–2% in measurement error. Only at very small strains occurring within the first or second 20  $\mu$ m increment of motion (at the beginning or end of our test) did these measurement errors exceed  $\sim 2\%$ , and never did they become greater than  $\sim 8\%$ . Consider the differences between *incremental* strains imposed by the micrometer ( $\Delta\epsilon_{mic}$ ) and measured by the optical system ( $\Delta\epsilon_{optical}$ ) for this test. These differences are a measure of the resolution of our system because they represent the error associated with detecting a 20  $\mu$ m actual motion. The average of the absolute values of the differences between these *incremental* strains is  $0.004 \pm 0.003\%$ . Since the initial gage length was 25.55 mm, this average per increment difference converts to  $\sim 1$   $\mu$ m. Recall that the resolution of our micrometer was 2  $\mu$ m, so it appears that errors reported in our optical system are *randomly* introduced from moving the blocks with the  $\pm 1$   $\mu$ m imprecision associated with using this micrometer [see Fig. 4(b)]. Further, at strains in the 0–11.74% range which were achieved by 100  $\mu$ m incremental motion, our system provided results that were *always* less than 2% in measurement error. Again, consider the differences between *incremental* strains imposed by the micrometer ( $\Delta\epsilon_{mic}$ ) and measured by the optical system ( $\Delta\epsilon_{optical}$ ) for this test [see Fig. 5(b)]. These differences are also check on the

Table 1. Biomechanical data from uniaxial tensile tests of rabbit calcaneus-Achilles tendon structures

Achilles tendon	Area (mm <sup>2</sup> )	Failure load (N)	Displacement (mm)	Stiffness (N mm <sup>-1</sup> )	Failure stress (MPa)	Failure strain (%)	Modulus (MPa)
Right (n=4)	5.4 $\pm$ 1.2	273.1 $\pm$ 29.0	4.46 $\pm$ 0.59	77.26 $\pm$ 6.18	51.8 $\pm$ 6.7	4.2 $\pm$ 0.5	1557 $\pm$ 396
Left (n=4)	5.0 $\pm$ 0.7	244.1 $\pm$ 75.8	4.48 $\pm$ 1.57	71.47 $\pm$ 7.14	49.2 $\pm$ 14.5	4.4 $\pm$ 1.2	1419 $\pm$ 337

Data reported as means  $\pm$  standard deviations.

resolution of our system because they represent the error associated with detecting a 100  $\mu\text{m}$  actual motion. Note that these incremental differences convert to  $\sim 1.7 \mu\text{m}$ , which is slightly larger than the differences expected due to random errors associated with imprecision in micrometer movement. Figure 5(b) suggests a potential bias of our system toward overestimating the increment of actual (micrometer) motion. Assuming the bias to be systematic error which is some percentage of total motion, it appears that when 20  $\mu\text{m}$  increments of motion are used the bias is not larger than the random imprecision associated with moving the micrometer whose resolution is 2  $\mu\text{m}$  [see Fig. 4(b)]. However, with the larger 100  $\mu\text{m}$  increments, this bias is larger than the random error and becomes evident [see Fig. 5(b)]. If future studies show this small bias is not negligible for practical purposes, the optical strain analysis software will be modified to compensate for this error. Also note that the percent measurement errors are reduced in the test using 100  $\mu\text{m}$  increments because the increment of motion is five times larger yet the differences did not increase proportionately. Hence the measurement errors are reduced.

Results from the calibration tests assess the optimal performance of our system since they are determined from ideal test specimens moving in a well-controlled manner. The largest sources of experimental error come from simple geometry effects of motions in/out of the plane of focus along the z-axis of the specimen and rotation about an in-plane axis perpendicular to the direction of strain. For the idealized calibration block used in our study, these rotational errors arose from a rotation about the vertical y-axis. However, it should be noted that if the direction of strain in a specimen is along the vertical y-axis in the xy-plane (as shown for the uniaxial tensile test depicted in Fig. 1), then large errors are introduced if that specimen rotates about the horizontal x-axis. Apparent strains due to motion in/out of the plane of focus can be minimized by positioning the camera as far from the object as possible. Note that we found the effects of lighting and lens  $f$ -stop on the results of linear motion in/out of the plane of focus (along the z-axis) to be insignificant over a range of  $f/4$  to  $f/16$ . As previously mentioned for nonidealized experimental tests, however, lighting should be adjusted to utilize a higher lens  $f$ -stop which will minimize apparent strains that arise from in/out of plane motion. Correction for optical distortion will eliminate errors that arise from the other translations. Errors resulting from rotation about an in-plane axis perpendicular to the direction of strain are the most troublesome since these rotations cannot be quantified, and only by rotating the camera with the object can they be minimized. Rotation about the z-axis perpendicular to the face of the object resulted in the development of significant apparent strains for large rotations. This was because the analysis software was initially written on the assumption that the region of interest was close to horizontal. Improvements to the software will provide our system with the ability to accurately measure strains across a region of interest oriented in any direction on the image.

Comparing the results of our *in vitro* biomechanical testing of rabbit Achilles tendon with data found for similar tissues suggests our system provides reasonable results and is an acceptable tool for measuring strains in soft biological tissues. In particular, in a study of rabbit tibial-MCL-femoral units, the failure strains were found to average  $7 \pm 1\%$  ( $n=10$ ) using the VDA system to measure tissue deformations (Woo *et al.*, 1983). Further, when normalized by cross-sectional area data reported for this tissue complex (Woo *et al.*, 1990), the failure loads reported by these authors suggest stress at failure to average about 60 MPa. In comparison, failure strains for the rabbit Achilles tendon-bone complex reported in the current study are in the 4–5% range, and failure stresses are approximately 50 MPa when using our optical system to quantify strains. Differences in the tissue and measurement technique are likely responsible for the variation in the data presented here.

We believe that our test conditions were such that uniaxial tension on the test specimen was achieved, and the specimen moved within the confines of acceptable motion for accurate strain measurement using our optical system's performance criteria. These experimental tests bought out many of the issues discussed above for evaluating tissue strains as well as few additional items. Typically, images from experimental tests have good contrast but are not perfectly sharp. Common imperfections include random markings, the effects of glare from the tissue surface, and the effects of a varying intensity of illumination over different areas of the tissue. In testing biological tissues such as tendon, where the surface strain is not uniform across the width of the tissues, the tissue may typically strain several percent uniaxially and often undergo significant other changes in shape such as tilting or twisting. Additionally, stretching of the tissue often stretches the lines, making them appear lighter, thus reducing the sharpness of an edge. Finally, calibration tests of linear in-plane motion of one block with respect to the other were run with the blocks submersed in a tank of circulating saline solution in order to evaluate the effects of the glass and liquid on optical measures. Results indicate that little or no optical distortion was introduced from the test tank or circulating fluid.

The optical system presented in this paper has some distinct advantages. The system is accurate and robust, finding the correct edges in all but occasional instances. Results indicate that the system can measure strains to within 2% measurement error for all strains in a 0–11.74% range when 100  $\mu\text{m}$  increments of motion are used. When a 20  $\mu\text{m}$  increment over 0–3.52% strain range is used, measurement errors exceed 2% only in the first or second increments of motion (at the beginning or end of the test) and never reach greater than 8%. As previously noted, these errors are representative of the resolution of the linear micrometer used for calibration. We acknowledge that in standard calibrating procedure, the accuracy of the calibration reference device should be at least one order of magnitude better than the device being tested. However, without *a priori* knowledge on the resolution of the optical system, and since there existed no other practical standards with resolution of a fraction of a micron, we were limited to the standards used. Hence, the resolution of our system appears to be as good as the micrometer (2  $\mu\text{m}$ ) but may actually have proved better if we had an even more precise calibrating standard available. In a calibration of the VDA for example, Lam *et al.* (1992) showed that system to be accurate to 10% measurement error over 10% strain. They state that deviations become increasingly large at lower strains using the VDA system. Our system is accurate to 0.05% strain at 3.52% strain and 0.18% strain at 11.74% strain. This range of strains is believed to include to physiological levels of strain in tendons and ligaments as well as the strains typically developed in *in vitro* uniaxial tension tests of tendon or ligament to failure. The current system also has the ability to track a region of tissue as it moves in the field of view. This feature provides maximum resolution and allows the measurement of strain over the same region of tissue on every frame. Additionally, the mathematical analysis software implemented by our system calculates the position of each edge of a stain line at 200–300 separate locations (each location representing one pixel) along the line depending on the size of the region of interest and then averages these positions to give the position of the line. This method is much more precise than a system that averages the image along the stain line *before* locating the edge. When the image is averaged before edge detection, the edges become blurred due to inexact vertical alignment which reduces the precision with which the distances between the edges can be measured. Alternatively, when the edge locations are determined and then averaged, numerous different measurements of the distance between the edges are averaged, resulting in increased precision. Other advantages of our system include the flexibility of being able to run more



than one analysis on the same set of images analyzing different regions of interest. Furthermore, this software can accurately measure strain across a region which has small angulations, irregularities, and waviness in the lines. With the exception of the video controller, the system uses standard equipment that might be found in any laboratory and is relatively inexpensive.

A unique feature of our system is use of a video controller and time-coded videotape. This allows the optical information to be simply and accurately interfaced with other data. Specifically, we can achieve precision synchronization of load-time and deformation-time results by electronically triggering the optical and mechanical testing systems to start data acquisition at the exact same time using the same electronic signal. Further, a frame address can be chosen corresponding to a specific point in time during a test. The video controller can then reproducibly find that exact frame to be digitized for analysis. Capturing images for analysis is completely automated using this frame addressing ability.

The primary disadvantage of our system is the post-processing time. Currently the region of interest and direction of strain are marked manually on each image. This procedure is time-consuming, but flexibility and accuracy are gained from manually selecting the same region of tissue on each image. Errors could potentially arise from not selecting the same region of interest on all images in a test series. When slightly different regions of tissue are analyzed on two images, even small differences in stain line architecture between the regions might induce apparent deformations. While these deformations are very small, they could represent large measurement errors for small strain calculations. These errors are minimal, however, relative to the same types of errors developed by overlaying a fixed window on the image. A final disadvantage is the limitation of our system to relatively slow strain rate tests (strain can be calculated at up to 30 time points per second).

In summary, the optical system developed in this laboratory has shown excellent performance in calibration tests. We believe that, within the guidelines described above, the system is a valuable tool for the measurement of strains in biological soft tissues. Besides its use in *in vitro* biomechanical tests, future applications implementing this system might include the measurement of *in vivo* surface strains in tendon during muscle contraction and a comparative study of internal tissue strains determined by an implantable transducer with surface strains determined by the optical system.

**Acknowledgements**—This work was supported by grants from the National Institutes of Health (AR-20557), the National Science Foundation, the Whitaker Foundation, the Bristol-Myers Squibb/Zimmer Orthopaedic Excellence Award, and the Department of Surgery at the University of Michigan. The authors additionally thank Dennis Kayner, Mark Stock, and Rick Zanecki for their contributions.

#### REFERENCES

- Amadio, P. C., Berglund, L. J. and An, K. N. (1992) Biochemically discrete zones of canine flexor tendon: evaluation of properties with a new photographic method. *J. orthop. Res.* **10**, 198–204.
- Arms, S., Boyle, J., Johnson, R. and Pope, M. (1983) Strain measurement in the medial collateral ligament of the human knee: an autopsy study. *J. Biomechanics* **16**, 491–496.
- Butler, D. L., Grood, E. S., Noyes, F. R., Zernicke, R. F. and Brackett, K. (1984) Effects of structure and strain measurement technique on the material properties of young human tendons and fascia. *J. Biomechanics* **17**, 579–596.
- Bulter, D. L., Sheh, M. Y., Stouffer, D. C., Samaranyake, V. A. and Levy, M. S. (1990) Surface strain variation in human patellar tendon and knee cruciate ligaments. *J. biomech. Engng* **112**, 38–45.
- Edwards, R. G., Lafferty, J. F. and Lange, K. O. (1970) Ligament strain in the human knee joint. *J. basic. Engng ASME* **92**, 131–136.
- Intaglietta, M. and Tompkins, W. R. (1972) On-line measurement of microvascular dimensions by television microscopy. *J. appl. Physiol.* **32**, 546–551.
- Kennedy, J. C., Hawkins, R. J. and Willis, R. B. (1997) Strain gauge analysis of knee ligaments. *Clin. Orthop. Rel. Res.* **129**, 225–229.
- Lam, T. C., Frank, C. B. and Shrive, N. G. (1992) Calibration characteristics of a video dimension analyser (VDA) system. *J. Biomechanics* **25**, 1227–1231.
- Lanir, Y. and Fung, Y. C. (1974) Two-dimensional mechanical properties of rabbit skin. I. Experimental system. *J. Biomechanics* **7**, 29–34.
- Lee, T. Q. and Danto, M. I. (1992) Application of a continuous video digitizing system for tensile testing of bone–soft tissue–bone complex. *Adv. Bioengng ASME* **22**, 87–90.
- Monahan, J. J., Grigg, P., Pappas, A. M., Leclair, W. J., Marks, T., Fowler, D. P. and Sullivan, T. J. (1984) *In vivo* strain patterns in the four major canine knee ligaments. *J. orthop. Res.* **2**, 408–418.
- Noyes, F. R., Butler, D. L., Grood, E. S., Zernicke, R. F. and Hefzy, M. S. (1984) Biomechanical analysis of human ligament grafts used in knee–ligament repairs and reconstructions. *J. Bone Jt Surg.* **66A**, 344–352.
- Ray, J. D., Feder, S. M., Butler, D. L. and Korvick, D. L. (1993) Simultaneous *in vivo* measurement of tendon force and strain in the goat model. *Trans. orthop Res. Soc.* **18**, 153.
- Roth, V. and Mow, V. C. (1980) The intrinsic tensile behavior of the matrix of bovine articular cartilage and its variation with age. *J. Bone Jt Surg.* **62A**, 1102–1117.
- Soslow, L. J., An, C. H., Johnston, S. P. and Carpenter, J. E. (1993) Geometric and mechanical properties of the coracoacromial ligament and their relationship to rotator cuff disease. *Trans. orthop. Res. Soc.* **18**, 139.
- Vanderby, R. Jr, Vailas, A. C., Graf, B. K., Thielke, R. J., Ulm, M. J. and Kohles, S. S. (1991) Acute effects of unweighting on the MCL–tibia insertion. *Trans. orthop Res. Soc.* **16**, 159.
- Woo, S. L. (1982) Mechanical properties of tendons and ligaments. I. Quasi-static and nonlinear viscoelastic properties. *Biorheology* **19**, 385–396.
- Woo, S. L., Akeson, W. H. and Jemott, G. F. (1976) Measurements of nonhomogeneous, directional mechanical properties of articular cartilage in tension. *J. Biomechanics* **9**, 785–791.
- Woo, S. L., Danto, M. I. and Ohland, K. J. (1990) The use of a laser micrometer system to determine the cross-sectional shape and area of ligaments: a comparative study with two existing methods. *J. biomech. Engng* **112**, 426–431.
- Woo, S. L., Gomez, M. A., Seguchi, Y., Endo, C. M. and Akeson, W. H. (1983) Measurement of mechanical properties of ligament substance from a bone–ligament–bone preparation. *J. orthop. Res.* **1**, 22–29.
- Yamamoto, N., Hayashi, K., Kuriyama, H., Ohno, K., Yasuda, K. and Kaneda, K. (1992) Mechanical properties of the rabbit patellar tendon. *J. biomech. Engng* **114**, 332–337.
- Yin, F. C., Tompkins, W. R., Peterson, K. L. and Intaglietta, M. (1972) A video-dimension analyzer. *IEEE Trans. biomed. Engng* **19**, 376–381.
- Zernicke, R. F., Butler, D. L., Grood, E. S. and Hefzy, M. S. (1984) Strain topography of human tendon and fascia. *J. biomech. Engng* **106**, 177–180.